DRIVERS AND ENVIRONMENTAL RESPONSES TO THE CHANGING ANNUAL SNOW CYCLE OF NORTHERN ALASKA

Christopher J. Cox, Robert S. Stone, David C. Douglas, Diane M. Stanitski, George J. Divoky, Geoff S. Dutton, Colm Sweeney, J. Craig George, and David U. Longenecker

On the North Slope of Alaska, earlier spring snowmelt and later onset of autumn snow accumulation are tied to atmospheric dynamics and sea ice conditions resulting in environmental responses.

Along the North Slope of Alaska (NSA), the annual cycles of environmental variables including wildlife behavior (e.g., Divoky et al. 2015; Liebezeit et al. 2014), biogeochemical cycles (e.g., Rhew et al. 2008; Sweeney et al. 2016; Zona et al. 2016), hydrology and hydroecology (e.g., Prowse et al. 2006), and vegetation (e.g., Bhatt et al. 2013) vary annually in response to seasonal warming and cooling of the surface, subsurface, and atmosphere. The timing of snow disappearance each spring influences the amount of solar radiation absorbed at the surface during May and June, and the associated variations in the net surface energy budget propagating downward through the subsurface affecting soil temperatures (e.g., Romanovsky et al. 2002; Westermann et al. 2009) and upward through the atmosphere, affecting air temperature and stability (e.g., Persson et al. 2002). Thus, the annual variability in the timing of snowmelt and length of the snow-free season significantly impact the Arctic terrestrial system as a whole.

AFFILIATIONS: Cox—Cooperative Institute for Research in Environmental Sciences, and Physical Sciences Division, NOAA/Earth System Research Laboratory, Boulder, Colorado; Stone—Science and Technology Corporation, and Global Monitoring Division, NOAA/Earth System Research Laboratory, Boulder, Colorado; Douglas—United States Geological Survey, Alaska Science Center, Juneau, Alaska; Stanitski—Global Monitoring Division, NOAA/Earth System Research Laboratory, Boulder, Colorado; Divoky—Friends of Cooper Island, Seattle, Washington; Dutton, Sweeney, and Longenecker—Cooperative Institute for Research in Environmental Sciences, and Global Monitoring Division, NOAA/Earth System Research Laboratory, Boulder, Colorado; George—Department of Wildlife Management, North Slope Borough, Utqiaġvik, Alaska
CORRESPONDING AUTHOR: Christopher J. Cox, christopher.j.cox@noaa.gov

The abstract for this article can be found in this issue, following the table of contents.
DOI:10.1175/BAMS-D-16-0201.1

A supplement to this article is available online (10.1175/BAMS-D-16-0201.2)

In final form 19 May 2017

The Arctic is undergoing unprecedented change. At few places is this more apparent than the North Slope of Alaska (NSA). The National Oceanic and Atmospheric Administration (NOAA) Global Monitoring Division (GMD) maintains an Atmospheric Baseline Observatory outside of Utqiaġvik (formerly Barrow) (71°19′23″N, 156°36′41″W) (Fig. 1) where a multidecadal trend toward earlier spring snowmelt and a lengthening snow-free season have been observed (Stone et al. 2002, 2005). This trend is broadly consistent with changes in snow cover variability in the Northern Hemisphere (Brown and Robinson 2011). Correlative relationships between the onset of melt over the sea ice in the nearby Beaufort and Chukchi Seas and the timing of the terrestrial growing season have also been identified (Stone et al. 2005; Bhatt et al. 2010).

Generally, springtime melting is forced by atmospheric longwave radiative processes, with shortwave processes largely acting as a feedback over both land (Wang et al. 2015) and sea ice (Persson 2012; Kapsch et al. 2013). In addition, cloud anomalies during the spring influence whether shortwave or longwave processes are dominant for a given year (Cox et al. 2016; Mortin et al. 2016). Recent warming of the permafrost (e.g., Shiklomanov et al. 2010) has prompted expectations for increased methane emissions from the tundra, but there is little evidence of this in the 30-yr record at the NOAA GMD observatory near Utqiaġvik (henceforth BRW) (Sweeney et al. 2016), opening questions about the pathways for transfer of carbon between the soil and the atmosphere. Changes in methane fluxes may be less likely to occur in summer, as previously thought, and more likely to occur during

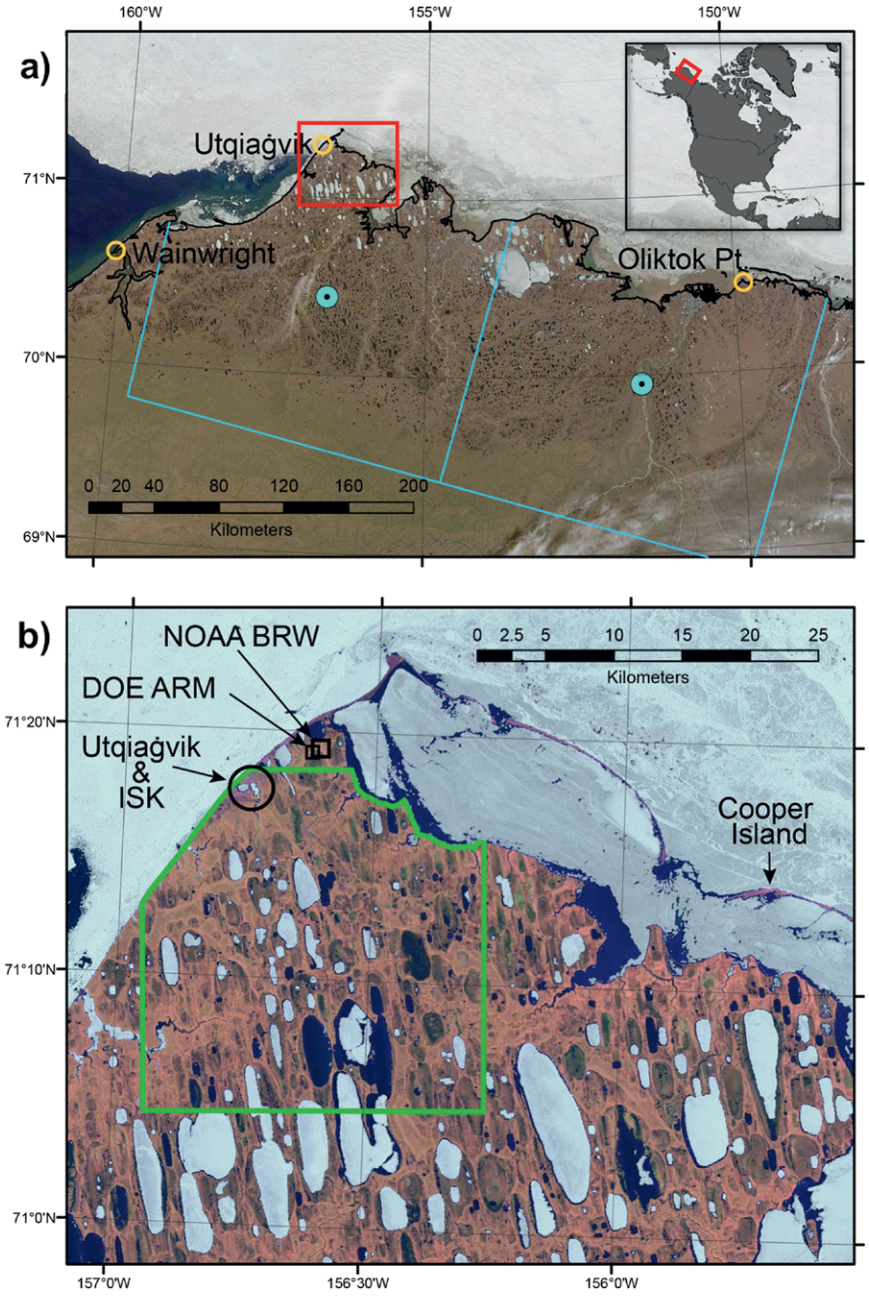

Fig. 1. (a) Broad-scale and (b) local-scale geographic setting of Utqiaġvik (formerly Barrow), Alaska, and the NOAA meteorological observatory. Comparative time series of snow cover extent (Estilow et al. 2015) and vegetation phenology (Didan and Barreto 2016) were extracted in the areas respectively delineated with (a) blue and (b) green polygons. Satellite images obtained by (a) MODIS (true color, 22 Jun 2015; NASA, https://worldview.earthdata.nasa.gov/) and (b) *Landsat-8* (false-color infrared, 21 Jun 2015; USGS, https://earthexplorer.usgs.gov/) show persistent lake and sea ice that are typical features in mid-June.

the cold season, in particular during the autumn freeze up (Zona et al. 2016). The freeze up is characterized by an extended "zero curtain" period during which the phase change in the moisture-laden soil maintains a nearly constant 0°C and is distinctly different than the springtime thaw that also involves latent heat exchanges but no pause during the transition from ice to liquid water (Outcalt et al. 1990). Other differences between the springtime melt and autumn freeze periods include differences in atmospheric and cloud properties (e.g., Shupe 2011; Shupe et al. 2011) and available sunlight.

An important atmospheric driver of early melt in spring is the advection of warm air across Alaska from the North Pacific (Stone et al. 2002, 2005; Graversen et al. 2011), which directly increases the downward longwave flux and modifies the turbulent sensible and latent fluxes (Kapsch et al. 2013). Such events have also been shown to affect the sea ice melt season by studies using both reanalysis data (Kapsch et al. 2013) and surface-based observations at Utqiaġvik (Dong et al. 2014; Cox et al. 2016). The amount of open water in autumn, in turn, is tied to warming of the Arctic's lower atmosphere, a process associated with Arctic amplification (e.g., Serreze et al. 2009 and references therein). Decreases in sea ice extent (Stroeve et al. 2012) have subsequently led to changes in polar bear distribution in late summer and autumn with some bears forced to terrestrial habitats on the NSA from their preferred sea ice (Atwood et al. 2016; Stern and Laidre 2016). Other species, including seabirds (Divoky et al. 2015) and marine mammals (Kovacs et al. 2011), also have to adapt to late summer and early autumn decreases in sea ice extent north of Alaska.

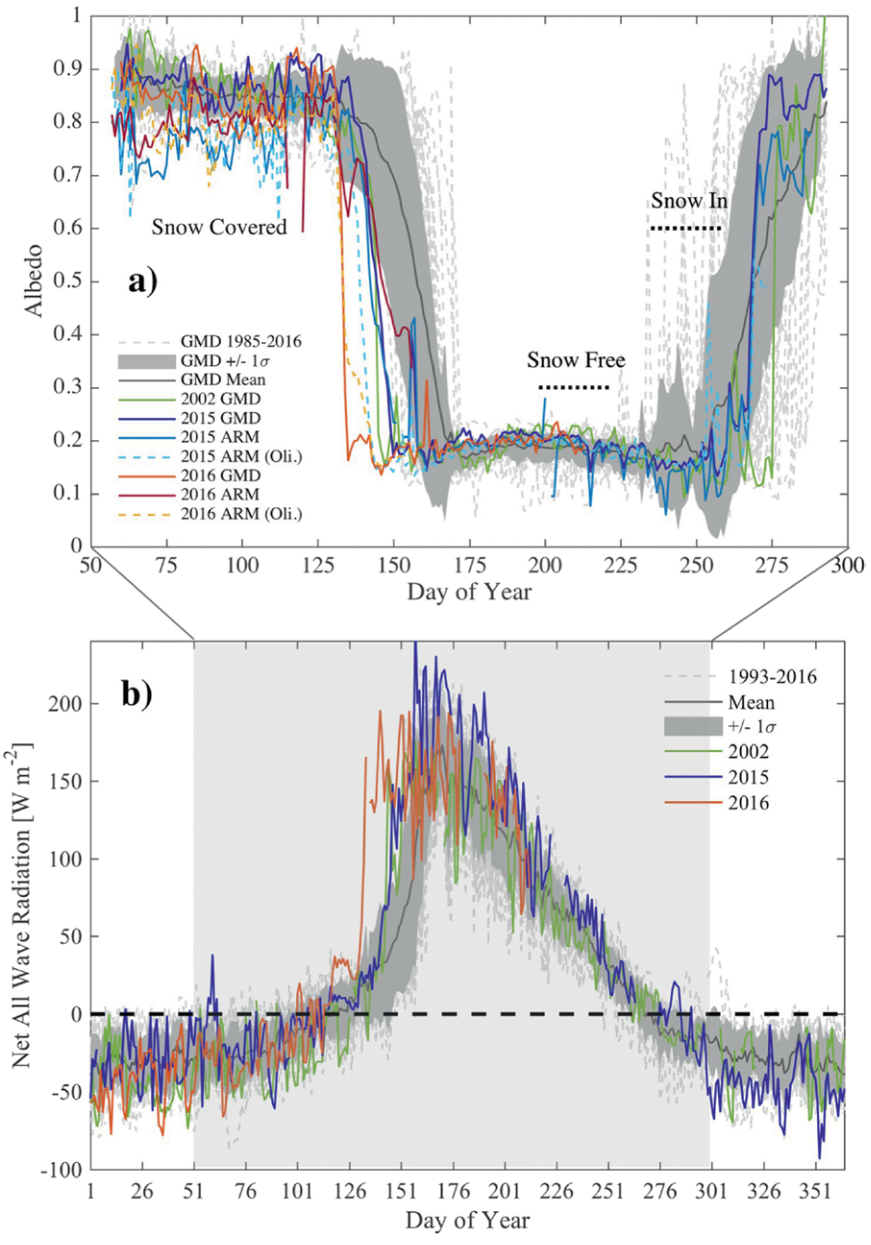

Fig. 2. (a) Daily mean albedo derived from broadband radiation measurements at BRW: 1987–2016 climatological mean (gray line) and standard deviation (gray area) and individual years for 2002 (solid green), 2015 (solid blue), and 2016 (solid orange). Also shown are analogous measurements for individual years made near BRW by ARM for 2015 (solid light blue) and 2016 (solid red) and Oliktok Point 250 km east of BRW for 2015 (dashed blue) and 2016 (dashed yellow). (b) Net all-wave radiation [(SW↓ − SW↑) + (LW↓ − LW↑)] measured at BRW denoted similarly to (top).

These findings warrant increased attention to coupled relationships within the atmosphere–

land–ice–ocean ecosystem in order to elucidate the mechanisms underlying the observed changes in any of these separate components (e.g., Uttal et al. 2016) and develop tools to predict future changes. This task is intrinsically interdisciplinary. Utqiaġvik is particularly well suited for observing the linkages between disparate environmental variables over long periods of time because of multidecadal climate monitoring supported by NOAA/GMD, NOAA/National Weather Service (NWS), the U.S. Department of Energy (DOE) Atmospheric Radiation Measurement (ARM) Program, the U.S. Geological Survey (USGS), and grant-funded and nonprofit projects in the vicinity (e.g., Hinkel and Nelson 2003; Divoky et al. 2015). Indeed, robust detection of the trends in snow cover at Utqiaġvik discussed here follows on a legacy of analysis and methodological development (Foster 1989; Dutton and Endres 1991; Foster et al. 1992; Stone et al. 2002, 2005; Hinzman et al. 2005; Hinkel and Nelson 2007).

The spring transitions from snow-covered to snow-free ground monitored at BRW were particularly early in 2015 and 2016, with anomalously warm temperatures leading to the fourth earliest date of snowmelt on record [day of year (DOY) 148, 28 May] and the record earliest date (DOY 134, 13 May) since the beginning of the twentieth century, respectively, while October 2016 tied 2012 for the warmest air temperatures on record at BRW, resulting in 2016 having the longest snow-free season yet observed. These events were driven by a variety of factors, leading to questions about whether 2015 and 2016 were highly anomalous or if they foreshadow a new norm. Using the seasonal cycle in snow cover as a synthesizing variable, this study expands upon Stone et al. (2002) to understand how measurements from Utqiaġvik during the twenty-first century fit into the context of those from previous decades. Focusing on both spring and autumn, the linkages between environmental responses and the atmospheric drivers that modulate the interannual variability in the timing and duration of the snow-free season are reported and discussed. The analysis is contextualized within both the long-term trends and recent anomalous events.

SNOW COVER AND THE SURFACE ENERGY BUDGET.

Determination of snow cover. Surface albedo quantifies the proportion of absorbed sunlight at the surface, measured as the ratio of reflected to incident broadband (295–2,800 nm) shortwave radiation. Because snow has a high albedo (0.8–0.9) and the underlying tundra has a low albedo (0.15–0.25), the timing of the seasonal cycle in snow cover can be inferred from albedos calculated from radiometric measurements (Fig. 2a). Following Stone et al. (2002), an albedo of 0.3 is used to identify the date when melt is complete; once albedo drops below 0.3 it rarely rises above for more than a day or so during episodic snowfall that can occur during summer. Alongside the climatology in Fig. 2a, three anonymously early years of melt are highlighted (2002, 2015, and 2016). The gentler slope of the climatological melting period in Fig. 2 (gray line and gray area) results from averaging many years. In fact, the rapid transitions of the highlighted years are typical; once melt begins in earnest it is complete within about 5 ± 2.4 days (1σ).

The radiometric measurements of albedo represent only the effective field of view of the downward-facing radiometer (tens of square meters). However, approximately 1 km southwest of BRW is the ARM observatory where similar radiometric measurements began in 1998. Melt dates at ARM are similar ($r = 0.69$, $p < 0.01$) but sometimes later than BRW because ARM is prone to accumulate drifting snow (Dong et al. 2010). While the 2015 ARM and BRW melt dates agree well, drift affected the ARM observations in 2016, possibly as a result of unusually strong and persistent winds during April ($r = 0.77$, $p < 0.001$ if 2016 is omitted). This level of correlation is generally repeated using radiometric data collected at Sagwon and Franklin Bluffs, approximately 350 km to the east (Stone et al. 2002), supporting the regional representativeness of BRW. Albedo measurements from the new coastal ARM Mobile Facility at Oliktok Point, approximately 260 km east of BRW, also show a similar snowmelt signal since installation in late 2013. Snowmelt data prior to the radiometric record were derived from a mixture of snow depth and temperature measurements (beginning in 1902) from the Weather Bureau/NWS (see Stone et al. 2002).

To further contextualize the snowmelt record from the Utqiaġvik area at regional scales, comparison is made to the Northern Hemisphere Snow Cover Extent (NH-SCE) dataset (Robinson et al. 2012), which is based on analysis of merged satellite products described in Estilow et al. (2015). To produce the NH-SCE time series for the NSA, snowmelt dates for two grid cells spanning the region slightly south and east of Utqiaġvik were averaged (see Fig. 1). The correlation between the BRW and NH-SCE melt dates is modest ($r = 0.6$, $p < 0.001$), but the mean, variance, and trend are similar, and many of the anomalous years are captured by both datasets (see Fig. ES1 of the supplement; https://doi.org/10.1175/BAMS-D-16-0201.2).

For the radiometric data, the snow-in date was identified as the day of year when albedo exceeded 0.6 and increased to sustained winter values. In spring the horizontal distribution of snow cover is more homogeneous than autumn and melting occurs relatively quickly and uniformly. Conversely, the autumn onset of snow accumulation is spatially more heterogeneous, including localized areas of snowfall, which sometimes melt again before persistent snow cover is established. In 2016, for instance, light snow fell by mid-October, but the tundra was not completely snow covered until early November, the latest snow-in date yet observed. Satellite-derived estimates (e.g., NH-SCE) of the snow-in date over the NSA are hampered by the high probability of cloud cover in autumn (~90% of the time; Shupe et al. 2011) and relatively low solar elevation angles that reduce the likelihood of satellite overpasses coinciding with sufficient illumination on the landscape. Consequently, the estimates of snow-in date between BRW and NH-SCE are uncorrelated (see Fig. ES2), although their agreement improves after the late 1990s when confidence in NH-SCE is higher (Estilow et al. 2015).

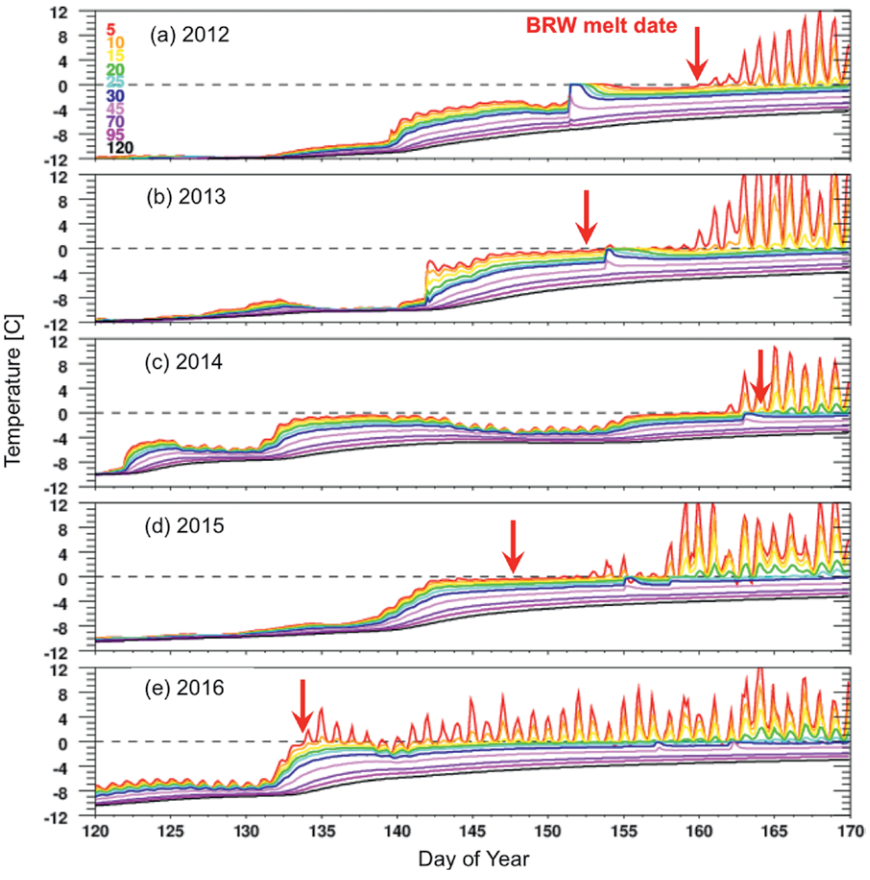

Fig. 3. Observed soil temperature at BRW from day of year (DOY) 120 to 170 at depths of 5 (red), 10 (orange), 15 (yellow), 20 (green), 25 (cyan), 30 (blue), 45 (pink), 70 (purple), 95 (magenta), and cm (black) from (a) 2012 through (e) 2016. Arrows show the date of snowmelt in each year at BRW.

Effect on the surface radiation budget and subsurface temperatures. The seasonal cycle in net surface radiation (Fig. 2b) is characterized by a net loss during winter when solar flux is negligible and a net gain in the summer when the albedo is low and the daily average solar flux is high. As a consequence of the large difference in albedo between snow and bare ground, the timing of snowmelt has an immediate and pronounced effect on the net shortwave flux at the surface, rapidly increasing the net radiative flux to large, positive values characteristic of summer (Fig. 2b). For the months of May and June, the additional absorbed radiation is ~1.9 W m^{-2} day^{-1} of advance of melt date (r = 0.85, p < 0.001). For context, the accumulated surface radiation is 406 MJ of absorbed energy at BRW in May and June on average, but in 2016, 674 MJ were absorbed.

The additional absorbed energy from earlier snowmelt may be redistributed and/or returned to the atmosphere in various ways over a range of time scales. The turbulent fluxes, which respond on the order of minutes to hours, likely compensate some proportion of the additional absorbed energy (Persson 2012; Sterk et al. 2013). Increased depth and temperature observed in the permafrost active layer suggest much of the energy is retained in the subsurface soils for months, while long-term changes in the permafrost temperatures in Alaska indicate that some amount of the storage may be decades or longer (Shiklomanov et al. 2010).

Spring soil temperatures at BRW, 2012–16 (Fig. 3), reveal the complexity and variability of soil temperatures in response to the timing of snowmelt (see also

sidebar "Seasonal biogeochemical cycles and snow cover"). Soil temperatures at all measured depths lead the date of snowmelt (denoted by arrows in Fig. 3) with the notable exception of 2016, when warming occurred simultaneously at all depths, consistent with a rapid and early rise in temperature. Following the loss of snow cover, a diurnal temperature cycle in the uppermost layers of the soil is established. The maximum active layer depth (ALD) that occurs later in summer was deeper in both 2015 and 2016 than in 2013 and 2014. However, in 2016 the ALD was slightly shallower than 2015 and was reached at an earlier date. While thawing at depth occurred earlier and faster in 2016 because of the early melt, it was later partially compensated by surface cooling owing to an increase in cloud cover during June and July, as evidenced by reduced net radiative flux during that time (Fig. 2b).

LONG-TERM TRENDS. *Snowmelt in spring and corroborative records.* A 115-yr climate record from Utqiaġvik shows a tendency toward earlier melt

SEASONAL BIOGEOCHEMICAL CYCLES AND SNOW COVER

The relationship between snow phenology and biogeochemical cycles on the tundra landscape varies depending on the chemical compound and its source–sink relationship, as highlighted by the example of methane (CH_4) and chloroform ($CHCl_3$). At BRW, a variety of natural and anthropogenic gases have been measured since the late 1970s. Observations of CH_4 began in 1986 and in 1999 the Chromatograph for Atmospheric Trace Species (CATS) added new capabilities including measurements of $CHCl_3$ (Hall et al. 2011). For these two gases, Fig. SB1 shows average (7-day smoothing applied) seasonal cycles at BRW of the enhancements above background, a proxy for the flux. The background is determined from samples collected when winds are blowing from the northeast (between 0° and 90°) across the neutral seascape (e.g., Sweeney et al. 2016). Enhanced mole fraction of both gases are observed during the snow-free period when the prevailing winds are from the south (150°–210°) across the tundra, beginning in spring, coincident with the onset of snow disappearance and onset of soil thawing (Fig. 3).

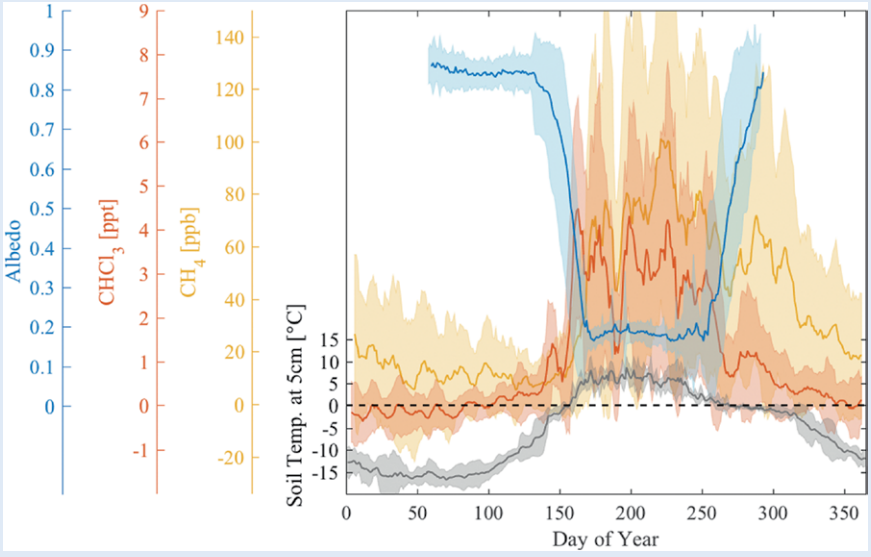

Fig. SB1. Multiyear composite seasonal cycles from BRW of albedo (1985–2016, blue), soil temperature at 5-cm depth (2012–15, gray), and enhancements above background levels of chloroform ($CHCl_3$) (1998–2015, red) and methane (CH_4) (1986–2015, yellow).

Enhancements of CH_4 continue through the autumn freeze-up period and beyond, when the moisture-laden soils maintain a near-constant temperature of 0°C (i.e., the "zero curtain"; Outcalt et al. 1990) and beyond (see also Fig. ES5). These cold-season CH_4 emissions may be 50% of the total CH_4 flux from the tundra for the year (Zona et al. 2016). Microbial activity in soil continues to produce CH_4 at low temperatures, near 0°C, or within a thin film of unfrozen water surrounding frozen soil (Zona et al. 2016). In either case, methane is released through the porous snow above.

Conversely, enhancements of $CHCl_3$ largely cease when snow begins to accumulate in autumn. Chloroform or trichloromethane is the second largest source of natural chlorine. More than half of $CHCl_3$ emissions are from natural sources (soils, biomass burning) (Silk et al. 1997; Khan et al. 2012) and the remaining anthropogenic sources include primary paper production and water treatment processes (Worton et al. 2006). The local lifetime of $CHCl_3$ is 149 days, thus limiting its influence on stratospheric chlorine and ozone (Carpenter and Reimann 2014). Naturally occurring tundra $CHCl_3$ emissions are persistent throughout the summer when little or no snow is present; however, it is not known if soil temperature or hydrology is the dominant driver for emissions. $CHCl_3$ is useful as a biogeochemical indicator, but the sources of $CHCl_3$ on the North Slope are poorly understood and therefore a better understanding of its regional role is needed to assess any potential implications of a longer snow-free period.

dates beginning around 1920, but not until after the mid-1970s was a statistically significant trend established (Fig. 4a) (–2.68 days decade^{-1}, 95% confidence interval, 1975–2016), a period that also represents the beginning of a warming trend in annual mean near-surface air temperature at BRW (Wendler et al. 2014). A deepening of the Aleutian low in 1976/77 (Trenberth and Hurrell 1994; Hare and Mantua 2000) promoted enhanced southerly flow over Alaska, which has been shown to contribute to earlier snowmelt at BRW (Stone et al. 2005).

In general, early snowmelt anomalies in Fig. 4a are larger deviations from the climatology (e.g., 10-yr running mean, yellow line) than late anomalies. This indicates a greater sensitivity to early melt than to preservation of the snowpack, which is likely an expression of the physical limit imposed on the persistence of snow under the influence of the annual solar cycle. The record earliest melt date occurred in 2016 (DOY 134), the second earliest in 2002 (DOY 144), and the fourth earliest in 2015 (DOY 148). The third earliest date of melt occurred in 1902 (DOY 145), the first year of the long-term record. The validity of this observation is supported by air temperature records that indicate a warming from below- to above-freezing temperatures just after this date (this is characteristic of the temperature response to the melt), and also by writings from James Wickersham in Nome, Alaska, on 7 and 11 May 1902, who noted the "beautiful spring weather" (Wickersham 1902, p. 7). While the 1902 observation indicates that the recent record-breaking years may not be unprecedented on century time scales, a modern departure from the historical baseline is evidenced by the fact that of the 10 melt dates taking place on or before DOY 155, 8 have occurred since 1990. As endpoints in the time series, the 2015 and 2016 anomalies exaggerate the magnitude of the trend since the mid-1970s (red line in the figure). Indeed, without 2015 and 2016, the recent trend toward earlier melt is less evident, perhaps related to another regime shift in the North Pacific in 1988/89 (Trenberth and Hurrell 1994; Hare and Mantua 2000). This regime shift represents a reversal of the late-1970s shift (Trenberth and Hurrell 1994). However, it is notable that the North Pacific index (Trenberth and Hurrell 1994) was also negative (a deeper Aleutian low) in the late 1990s and 2000s until a brief reversal centered on 2010 (Hurrell 2017).

The post-1975 BRW snowmelt dates from Fig. 4a are reproduced in Fig. 4b (bold black line) together with several other corroborating metrics of climate-sensitive environmental indicators near Utqiaġvik.

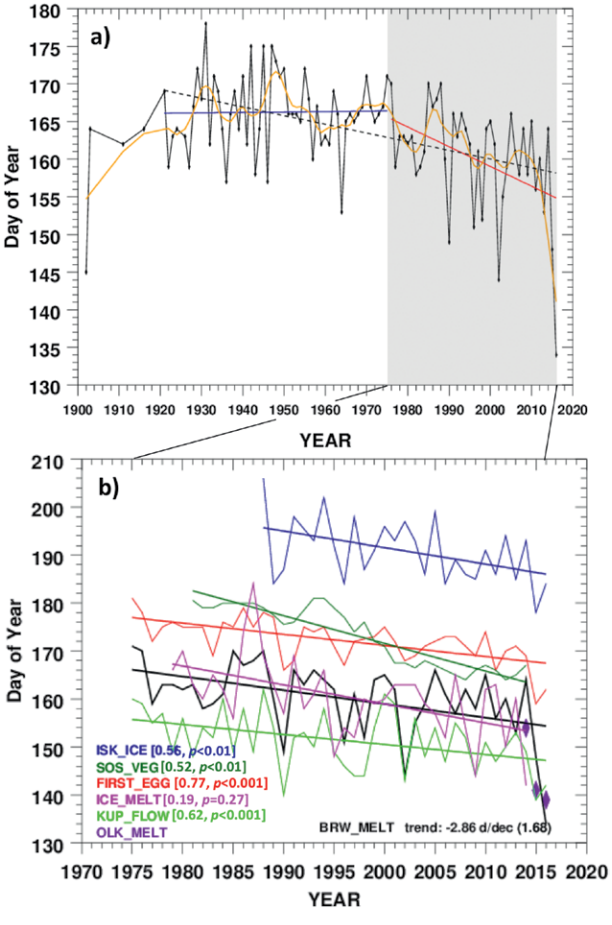

Fig. 4. (a) Time series of snowmelt dates at BRW ("BRW_MELT"); orange line is a 10-yr running mean and linear fits are shown for 1920–75 (blue), 1920–2016 (dashed), and 1975–2016 (red). (b) Reproduction of the 1975–2016 snowmelt dates shown in (a) (bold black line) alongside several other environmental metrics that benchmark the onset of spring in nearby areas: ice-out date in Isaktoak Lagoon (ISK_ICE) (1988–2016, missing 1992), onset of flow >10,000 cfs in the Kuparuk River (KUP_FLOW) (1975–2016), start of the vegetation growing season derived from NDVI smoothed with a 3-yr running mean (SOS_VEG) south of BRW (see Fig. 1b) (1981–2014), date of first black guillemot egg on Cooper Island (FIRST_EGG) (1975–2016, missing 1998), and the mean melt onset date over the sea ice (first liquid water in the snow or on the surface of the ice) in the region north of Utqiaġvik (70°–75°N, 165°–140°W, shown in Fig. SB2d) (ICE_MELT) (1979–2014). Recent snowmelt dates at Oliktok Point, Alaska, are shown with diamonds. Correlations (Pearson product moment) with BRW snowmelt dates are shown in brackets. The value in parentheses is the uncertainty in the snowmelt trend at the 95% confidence interval. BRW_MELT was first smoothed with a 3-yr running mean before being correlated with the similarly smoothed SOS_VEG.

Annual onset dates of the vegetation growing season south of Utqiaġvik (see Fig. 1b), derived with the normalized difference vegetation index (NDVI; Tucker 1979) from daily satellite imagery (Didan and Barreto 2016), have trended toward earlier dates and covaried with the BRW snowmelt dates (see also sidebar "Regional changes in vegetation phenology and sea ice dynamics"). The ice-out date in the freshwater Isaktoak Lagoon adjacent to Utqiaġvik has also trended earlier at a similar rate with snowmelt, but about a month later owing to the large volume of ice that must completely melt. The date at which streamflow first reached 10,000 cubic feet per second (cfs; ~283 $m^3 s^{-1}$) at the mouth of the Kuparuk River near Deadhorse (~300 km east of BRW) also tracks the snowmelt date at BRW, as did recent radiometric measurements of albedo at Oliktok Point (described earlier).

To relate the BRW snowmelt record to sea ice (see also sidebar "Regional changes in vegetation phenology and sea ice dynamics"), a mean date was calculated for each year, 1979–2016, when surface melt on the sea ice was first detected in passive microwave satellite observations (Markus et al. 2009) within an adjacent offshore region encompassing 70°–75°N and 165°–140°W (shown in Fig. SB2a). The sea ice melt onset metric has a similar trend to BRW snowmelt, but the correlation is not significant (Fig. 4b). Stone et al. (2005) reported a correlation between BRW snowmelt and the onset of ice melt, but the correlations were concentrated in the East Siberian and western Chukchi Seas and not the Beaufort Sea where the sea ice time series shown in Fig. 4b was quantified. This spatial variability may be associated with atmospheric circulation patterns that are discussed in the following section.

REGIONAL CHANGES IN VEGETATION PHENOLOGY AND SEA ICE DYNAMICS

The earlier snowmelt and longer growing season trends observed at BRW (Figs. 4 and 5) represent changes that are taking place throughout eastern Russia and Alaska specifically (Fig. SB2) and across the Northern Hemisphere in general. Northern Hemisphere snow cover extent in June, when snow is mostly restricted to the Arctic, has declined by nearly 18% $decade^{-1}$ since 1979 (Derksen and Brown 2012). The nonfrozen season for land north of 45°N latitude has lengthened by 2.4 days $decade^{-1}$ (Kim et al. 2014). In the Pacific Arctic (Fig. SB2), both earlier melt and later freeze, accompanied by unprecedented losses in summer sea ice, have contributed significantly to lengthening the snow-free period (refer also to section "Onset of snow accumulation in autumn and end-of-season metrics" in the main text).

Onset of the Arctic growing season is primarily constrained by temperature (Kim et al. 2014) so it is coupled to the same mechanisms that melt the snowpack (Mioduszewski et al. 2015; Li et al. 2016). While a number of studies document a trend toward longer growing seasons at high northern latitudes, the relative contributions of earlier start dates versus later end dates differ regionally (Zeng et al. 2011; Bieniek et al. 2015). Shifts toward both earlier start dates and later end dates, however, underlie the longer growing season observed across most of the Pacific Arctic as illustrated in Fig. SB2.

Start of the melt season on sea ice north of Utqiaġvik has also trended earlier (Fig. SB2d) by 4.3 days $decade^{-1}$ from 1979 to 2014 ($r^2 = 0.23$, $p < 0.01$). The melt onset detection method is sensitive to the first appearance of liquid water in either snow or on the sea ice surface, which generally happens before the nearshore terrestrial snowpack disappears and well before the sea ice itself melts. The earlier melt and green-up trends in the Arctic are primarily driven by rising air temperatures (Zhu et al. 2016), which are in turn are associated with regional circulation patterns that favor advection of warm air and moisture from the North Pacific during late winter or early spring (Stone et al. 2005; Semmens et al. 2013; Mioduszewski et al. 2015; Mortin et al. 2016; this study).

End-of-season trends in Pacific Arctic phenology are linked to the distribution of sea ice and timing of ice formation. In the ocean north of Utqiaġvik, the linear trend in median freeze onset date during 1979–2014 was 16.5 days $decade^{-1}$ ($r^2 = 0.55$, $p < 0.001$). During 1982–99, sea ice formation immediately north of Utqiaġvik occurred at roughly

Fig. SB2. Median start and end dates of the vegetation growing season, and the sea ice melt/freeze season, during (a),(d) 1982–99 and (b),(e) 2000–14 throughout the Pacific Arctic. Start and end dates of the vegetation growing season were calculated using phenology metrics derived from NDVI (Didan and Barreto 2016). Sea ice melt onset and freeze onset dates were calculated using metrics derived from passive microwave brightness temperatures (Markus et al. 2009). Median edge of the pack ice (>15% ice concentration from Cavalieri et al. 1996) is shown (bold white line) for (a),(b) 1 Jun and (d),(e) 1 Oct. Profiles of median (c) start of season and (f) end-of-season dates are shown along a longitudinal (156.5°W) transect spanning 60°–76°N shown in (a), which passes through Utqiaġvik at the land–ocean interface. The offshore polygon in (d) delineates where ICE_<MELT, FREEZE> (Figs. 4b and 5a) and ICE_EOS (Fig. 5b) were calculated.

The congruent trends and covariations between the timing of snowmelt and the onset of hydrological and biological processes illustrate the broad influence that spring weather conditions have on Arctic ecosystems (see also sidebar "Ecological responses to changing seasonality"). At a nesting colony of Mandt's black guillemots (*Cepphus grylle mandtii*) on nearby Cooper Island (Fig. 1b), egg laying has trended earlier and covaried closely with the snowmelt dates at BRW ($r = 0.77$, $p < 0.001$). Female guillemots do not ovulate until they have access to a ground-level nest cavity, which they are prevented from entering until the snow has cleared; then they typically lay two eggs per nest per year (Divoky et al. 1974). The breeding colony at Cooper Island was first discovered in 1972 inhabiting wooden structural debris littered on the island, and since 1975, comprehensive records have been kept of the colony's nesting ecology (Divoky et al. 1974, 2015). The date of the first egg has advanced 2.6 ± 0.8 days decade^{-1} (95% confidence interval), and the median date of egg laying (not shown) has advanced 2.4 ± 0.6 days decade^{-1} (95% confidence interval). Similar advancements have been observed for bird species breeding on the adjacent coastal tundra (Liebezeit et al. 2014). In 2016, the appearance of first egg was slightly later than 2015, but the median date of egg laying (and thus, the breeding season) was the earliest on record (DOY 168) by 3 days (Fig. SB4). Early nesting is important for the guillemots to fledge their young before the extensive loss of sea ice north of Utqiaġvik, now common by August (see sidebar "Black guillemots of Cooper Island"). Other anomalous snowmelt years (e.g., 1990, 2002, 2015) were also early years for the appearance of first egg, but less extreme than the snowmelt anomalies. This suggests that factors such as increased risks of predation (due

the same time the growing season ended but since has occurred later by several weeks (Figs. SB2c and SB2f). As discussed in the main text, greater solar heating of the open ocean water during summer and delayed ice formation in autumn underlies the persistent rise in October and November air temperatures at BRW.

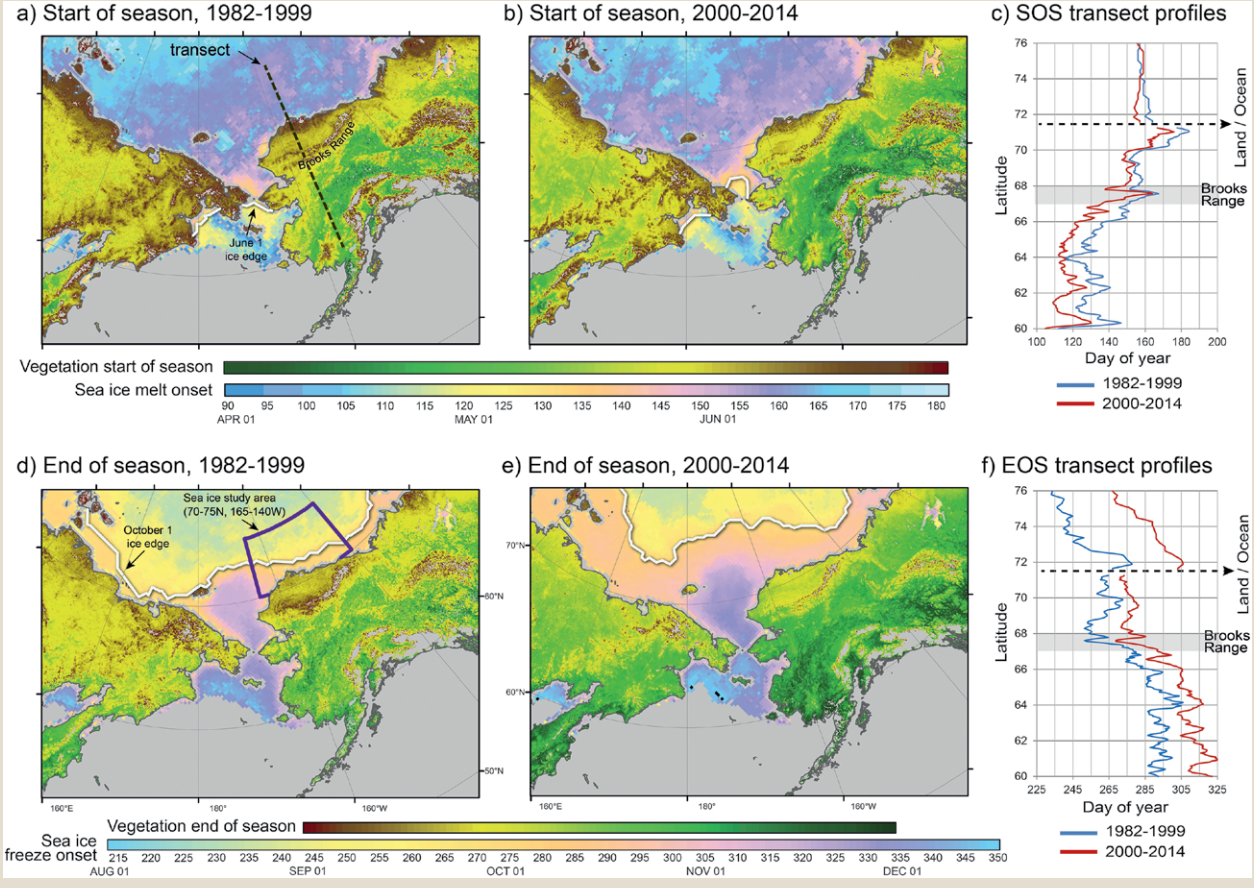

to a lack of open water) or loss of access to eggs from late snowfall may be important in natural selection, deterring extreme early breeding.

Onset of snow accumulation in autumn and end-of-season metrics. Figure 5a shows end-of-season metrics for a set of measured variables that are used here as proxies of the onset of winter. The timing of end-of-season is observed, in general, to be later in the post-2000 time period than during the 1980s and 1990s. The sea ice freeze onset date in the offshore region north of BRW and the end of vegetative growing season are both correlated with the date of snow-in at BRW (black line, Fig. 5a). Note that all of these metrics show some evidence of a regime shift around the year 2000.

Warming of the Arctic is occurring faster than at lower latitudes, is more pronounced in autumn, and is accompanied by larger and more persistent areas of ice-free ocean (Serreze et al. 2009). The impact of extensive sea ice retreat in the Beaufort Sea on northern Alaska temperatures, particularly during October, is highlighted in Wendler et al. (2010, 2014). Following a somewhat similar methodology to the studies by Wendler et al., the relationship is quantified here between mean October air temperature at BRW and the date that autumn sea ice extent first covered >60% of the offshore region previously defined in Fig. 4b. The remarkably high correlation ($r = 0.91$, $p < 0.001$, Fig. 5b) gives evidence that the delay in freezing of the ocean north of Alaska imparts a strong influence on autumn temperatures at Utqiaġvik,

ECOLOGICAL RESPONSES TO CHANGING SEASONALITY

All living components of the Arctic ecosystem—plants, animals, and humans—possess strategies that are tuned to the region's extreme seasonality. As the Arctic warms and seasonal trends emerge, the adaptive capacities of those strategies become tested. Throughout the food chain, grazers, insectivores, and predators are challenged to maintain alignment with spatial and temporal changes in the availability of their food resources. Misalignment, or trophic mismatch (Durant et al. 2007), can be especially detrimental to reproduction.

Many Arctic birds are migrating earlier, although some species have not kept pace with the rates of environmental change (Ward et al. 2016). Geese are observed to fledge fewer goslings in years with greater mismatch between nesting dates and vegetation phenology, especially when eggs hatch late (relative to the vegetation) and young growing birds are deprived of the seasonal peak in high-quality forage (Brook et al. 2015; Doiron et al. 2015). Caribou calves <1 month in age, however, have higher survival rates in years with earlier snowmelt (Griffith et al. 2002), although all resident grazing species in the Arctic (e.g., caribou, reindeer, muskox, voles, etc.) are vulnerable to rain-on-snow events during winter that can render their forage inaccessible (Stien et al. 2012; Forbes et al. 2016).

Offshore, earlier trends in sea ice melt onset (Stroeve et al. 2014) have contributed to unprecedented sea ice losses in late summer, which in turn have altered the seasonal habitat conditions of marine mammals like polar bears, walruses, whales, and ice seals (Moore and Huntington 2008), and the seasonal hunting conditions of native residents who depend on those animals for food and culture (Cochran et al. 2013). Stationary sea ice abutting the coast (shorefast ice) is commonly used by coastal residents for hunting camps and transportation routes; however, Arctic warming has made that ice less predictable and thus more risky to occupy (Druckenmiller et al. 2010).

Sea ice loss has caused more polar bears to come ashore during summer (Atwood et al. 2016; Rode et al. 2015b), limiting their access to food (Rode et al. 2015a) and elevating their risk of encountering humans. On Cooper Island, site of a long-term black guillemot study (see next sidebar), polar bears have become common late-summer visitors (Fig. SB3) since the sea ice began melting more extensively over the polar bear's preferred continental-shelf hunting grounds (Durner et al. 2009).

Rapid warming of the Arctic ecosystem has imposed, and will continue to impose, challenges and opportunities to its current and future inhabitants. Recognizing the present and likely future rates of anthropogenic climate forcing, ecological balance in the Arctic will be many decades—possibly centuries—in the making.

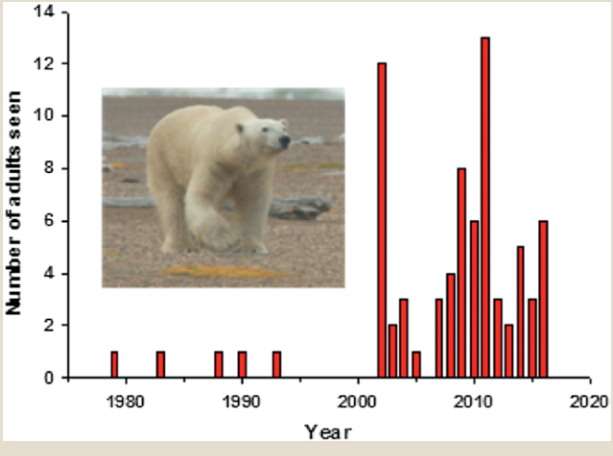

Fig. SB3. Number of unique adult polar bears sighted on Cooper Island each year during late summer, 1975–2016.

noting that the prevailing October onshore winds are from the east-northeast (onshore) and that Utqiaġvik is a coastal location. The early onset of spring sea ice melt promotes more extensive summer sea ice retreat in the Chukchi and Beaufort Seas, which acts to postpone autumn ice formation (Markus et al. 2009; Stroeve et al. 2014) with a positive feedback on autumn air temperatures over the NSA, thereby also extending the snow-free season. Notably, however, the trend is weaker after ~2000 (Fig. 5b). It remains to be seen whether this represents a brief pause in October warming at Utquaġvik or is an indication of the influence of the freezing of the ocean, reducing the supply of warm air for advection landward and keeping air temperatures close to the freezing point of seawater. This would explain why the variance in the sea ice and temperature records is smaller in recent years, potentially reaching a limit where the loss of sunlight leads to rapid longwave cooling of the surface and ice formation. However, with added greenhouse gas forcing, model projections of future winter sea ice suggest that energy absorbed into the Arctic Ocean or transported by currents from lower latitudes can sustain open water well into November (Wang and Overland 2015). In fact, presently, average November temperatures at BRW show a significant increasing trend (see Fig. ES3).

DRIVERS OF VARIABILITY. Stone et al. (2002) described several influential factors associated with the date of snowmelt at BRW: the amount of snowfall in the preceding winter (expressed as water equivalent) and, from March through May, the air temperature and cloud cover (which modulates the surface radiation balance). That study reported a decrease in October–February water equivalent precipitation (WEPC) from 1966 to 2000 and increasing springtime air temperatures and cloud cover over the same time period. The combination of these factors was implicated in explaining the observed trend in snowmelt date.

THE BLACK GUILLEMOTS OF COOPER ISLAND

Mandt's black guillemot (*Cepphus grylle mandtii*), one of the few seabirds associated with sea ice year-round (Divoky et al. 2016), breeds on shorelines adjacent to ice in summer and has been studied at Cooper Island since 1975. The species first benefitted from warming during the twentieth century but has since been negatively affected. Black guillemot's require a snow-free nest cavity for a minimum of 80 days for successful nesting, so the species was unable to colonize northern Alaska until the late 1960s and early 1970s (Divoky et al. 1974; MacLean and Verbeek 1968) when the annual snow-free period began to regularly exceed 80 days, as it has every year since, except in 1988 when persistent snow accumulations impacted chick survival (Divoky 1998) (Fig. SB4).

While increasing atmospheric temperatures have provided an earlier and longer breeding season for Mandt's black guillemots in Arctic Alaska, a corresponding loss of summer sea ice in the region has also occurred. The increased distance from Cooper Island to the ice pack during the period of chick rearing has reduced accessibility to their preferred ice-associated prey, Arctic cod, resulting in starvation of chicks and low fledging weights (Divoky et al. 2015). Less sea ice has also resulted in increased occurrences of a nest predator, the polar bear (Fig. SB3), and a nest competitor, the horned puffin, both of which reduced black guillemot hatching and fledging success until the wooden debris originally used as nest sites was replaced in 2011 with plastic bear- and puffin-proof nest cases (see inset in Fig. SB4a). Decreased breeding success at the Cooper Island colony coupled with decreased immigration (indicating poor productivity at other colonies) has resulted in the Cooper Island population of guillemots dropping from a peak of over 200 pairs in 1989 to 100 pairs in 2016. Similar changes in prey and colony size have been observed at a black guillemot colony in the eastern Beaufort Sea (Government of Yukon 2015).

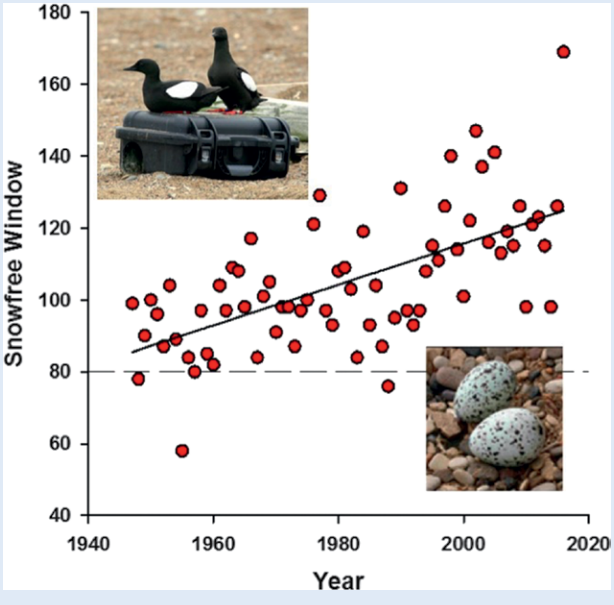

Fig. SB4. Duration of annual snow-free period at Utqiaġvik, from spring snowmelt to >2.5-cm autumn accumulation (data: National Weather Service). Black guillemots require at least 80 snow-free days (dashed horizontal line) for nesting. Inset images show (top left) a breeding pair on one of the bear-proof nesting containers and (lower right) an example of black guillemot eggs.

A reexamination using updated records (Fig. 6) reveals a modest increase in WEPC after 2000, reversing the pre-2000 trend discussed also by Curtis et al. (1998). This has important implications. First, the observed decrease in WEPC reported by Stone et al. (2002) is seen to be compensated by increases since ~2000 and is not observed in the expanded record to explain the trend in spring snowmelt as earlier indicated. Additionally, the updated analysis of WEPC measured at BRW shows no correlation with the melt date there (Fig. 6). Thus, the winter snowfall amount does not appear to play a significant role in determining the interannual variability in the timing of snowmelt at BRW. Indeed, both the 2015 and 2016 melt-date anomalies occurred in years with unremarkable or slightly above-normal wintertime precipitation. Anomalously high winds recorded during April in 2016 (Fig. ES4) are consistent with the hypothesis that the early snowmelt in 2016 may have been partially facilitated by sublimation in early spring. However, analysis of BRW snow depth measurements does not support this, showing rather that melt occurred quickly and was not preceded by a slow decrease in the snowpack, implicating instead a heat wave that affected much of Alaska during May.

Trends in air temperature in March–April and May are significantly correlated with melt date at BRW (Fig. 6), consistent with 2016 observations and prior work. The air temperature may be modified by local variations in the surface energy budget, such as those forced by clouds, and/or by advection of air masses from elsewhere. The amount of cloud cover is only weakly correlated with melt date in March and April and uncorrelated in May. The influence of Arctic cloud cover on near-surface air temperature is well documented (e.g., Stone 1997) and cloud cover was earlier found to be correlated with melt date between 1966 and 2000 (Stone et al. 2002). The results here indicate greater influence of warm-air advection during May at BRW since 2000 than previous analysis revealed. Furthermore, advection of warm air is the dominate factor because cloud radiative forcing at Utqiaġvik during May is neutral to positive, becoming larger and negative in June when clouds tend to cool the surface in response to decreasing surface albedo and increasing solar elevation angle (e.g., Dong et al. 2010; Cox et al. 2016).

The underlying drivers of the conditions that promote melt or preserve snow locally at Utqiaġvik include atmospheric circulation patterns in the North Pacific and Beaufort Sea regions, which either enhance or block exchanges of energy and moisture between lower latitudes and the Arctic in the vicinity of Alaska and the Bering Strait (e.g., Stone et al. 2002, 2005; Graversen et al. 2011; Dong et al. 2014). Using 850-hPa geopotential height fields (March–May, 1948–2016) from the NCEP–NCAR reanalysis (Kalnay et al. 1996), the relationship is examined here between the date of snowmelt in spring at BRW and variability in the two dominant atmospheric circulation patterns affecting northern Alaska and the adjacent seas, the Aleutian low and the Beaufort high, specifically the strength and direction of the

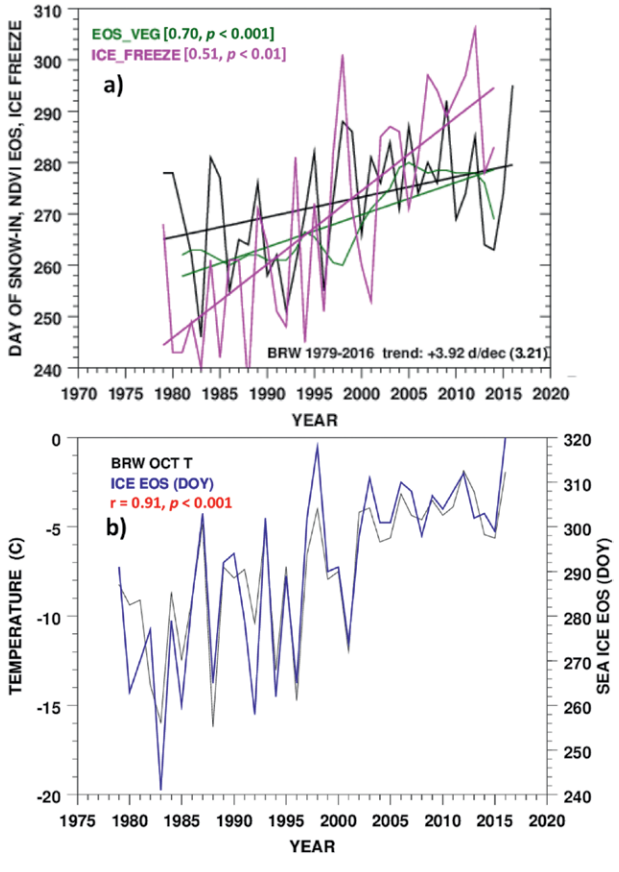

Fig. 5. (a) End-of-season (EOS) metrics; timing of establishment of seasonal snowpack at BRW (black line), end of the vegetation growing season derived from NDVI (smoothed with a 3-yr running mean) (EOS_VEG) (1981–2014) just south of BRW (see Fig. 1b), and mean sea ice freeze onset date (ICE_FREEZE) (1979–2014). Correlations (Pearson product moment) with BRW snowmelt dates are shown in brackets. The value in parentheses is the uncertainty in the trend at the 95% confidence interval. The BRW record in (a) was first smoothed with a 3-yr running mean before being correlated with the similarly smoothed EOS_VEG. (b) October mean 2-m air temperature at BRW (black) and date when autumn sea ice extent first attained >60% coverage of an area north of Utqiaġvik (70°–75°N, 165°–140°W).

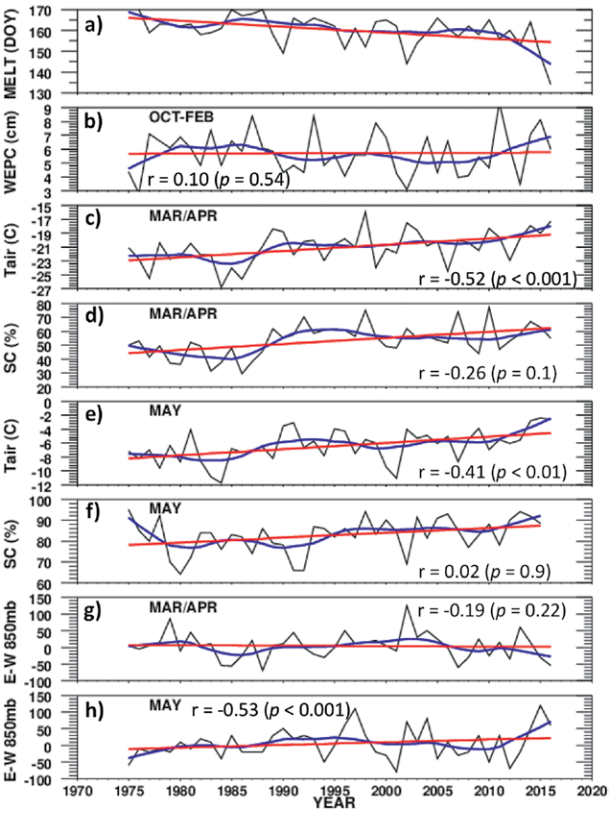

Fig. 6. (a) Date of snowmelt at BRW 1975–2016; (b) WEPC mean Oct–Feb; (c) BRW 2-m air temperature mean Mar–Apr; (d) total sky cover (SC) mean Mar–Apr; (e) as in (c), but for May; (f) as in (d), but for May; (g) EW 850-hPa geopotential heights, where E is 55°N, 150°W and W is 55°N, 160°E for Mar–Apr; (h) as in (g), but for May. In (b)–(h), Pearson correlations *r* between the variable shown in the panel and the date of snowmelt in (a) are shown. For each panel, a LOWESS smoothed fit using a 10-yr filter (blue) and linear fit (red) are also shown.

anomaly in the meridional [north minus south (NS)] 850-hPa geopotential height gradient and the relative zonal position of the Aleutian low and higher pressure observed to the east [east minus west (EW)] (Fig. 7a). The former describes the tendency for the atmosphere to support or block exchanges of air masses between the North Pacific and the Arctic, while the latter relates to the potential for advection of warm, moist air from the North Pacific into the Arctic. The strength of the NS dipole pattern appears to be relatively insignificant (not shown), while EW appears influential, in particular during May (Figs. 6 and 7). It is apparent from the magnitude of the departure from the mean (black contour lines in Figs. 7a–c) that this pattern is particularly influential for early years and less influential for late years. Interpretation of this relationship is complicated by the fact that the correlation between EW in May and snowmelt at BRW appears to be an emergent feature (Fig. 7e), beginning sometime in the mid-1970s and becoming steadily larger and more significant during the 1980s, possibly following the shift in atmospheric circulation in 1977 discussed earlier. This emergence does not appear to be a feature of the trends themselves, however, because the relationship remains unchanged when the analysis is repeated using a linearly detrended time series (dashed lines in the figure). The apparent increase in the importance of advection is consistent with a relative weakening of the influence of cloud forcing, though cloud properties in the far western Arctic and southerly advection have also been linked by several studies (e.g., Kapsch et al. 2013; Dong et al. 2014; Cox et al. 2016), opening questions about how the characteristics of these events may lead to different responses within the Arctic.

A more detailed evaluation of the time series of the EW index (not presented here) shows that advection of southerly air in May was an important factor in the recent snowmelt anomalies in 2015 and 2016, with an enhanced EW dipole favoring the flow of warm air across Alaska into the Arctic. Warmer than average SSTs in the Gulf of Alaska in 2015 and 2016 may have further added to the heat waves experienced at Utqiaġvik, as air circulating around the Aleutian low would have crossed a region of abnormally warm water in those years referred to as the "blob" (Fig. 7d) (Bond et al. 2015; Kintisch 2015; Amaya et al. 2016), which formed in 2013 but recurred in subsequent years. Indeed, positive anomalies in latent heat flux are observed in the region of the blob in the NCEP–NCAR reanalysis during May of both years (compared to the 1979–2016 May average) (not shown). In 2013 and 2014, the blob formed as a pool of anomalously warm water in the Gulf of Alaska region, observed in association with a persistent ridge pattern that is consistent with a positive EW index, a scenario that was also seen to incite resurgence from one year to the next as a result of possible teleconnections with the tropics (Di Lorenzo and Mantua 2016). The correlation *r* between EW and SST in the Pacific (10°–62°N, 110°W–180°, following Di Lorenzo and Mantua 2016) during May 1975–2016 is 0.59 ($p < 0.001$), indicating that the dominant pattern supporting southerly flow from the North Pacific into Alaska is generally associated with anomalously warm waters in the region. While these two characteristics are not independent, the result does point to a combination of influences supporting heat waves that impact the Alaskan Arctic. Furthermore, the EW index is correlated with

the Niño-3.4 SST index for ENSO during May (r = 0.46, $p < 0.01$). These findings are consistent with the conclusion of Di Lorenzo and Mantua (2016), who hypothesized that tropical teleconnections were significant in the anomalies observed in the North Pacific in 2013 and 2014. Thus, the relatively small correlation observed between ENSO in May and the timing of the snowmelt at BRW (r = –0.28, $p < 0.1$) may implicate an indirect influence of ENSO on the NSA during spring via teleconnections.

SUMMARY AND FUTURE DIRECTIONS. The seasonal cycle of snow cover along Alaska's northern coast is used here as an integrating variable linking large-scale circulation anomalies to local processes and the associated responses in biogeochemical cycles, wildlife behavior, and vegetation phenology. A continuation of previously reported trends toward early spring snowmelt at Utqiaġvik (formerly Barrow) is documented with the fourth (DOY 148) and first (DOY 134) earliest dates on record occurring in 2015 and 2016, respectively. Additionally, the arrival of an established snowpack in autumn is found to be occurring later and, thus, taken together, a dramatic lengthening of the snow-free season has emerged. The duration of the snow-free season was particularly anomalous in 2016 (45% longer than the 1975–2015 average) because both the earliest melt and latest persistent snow cover on record (DOY 295) occurred in the same year. The latest date for the onset of freezing at Isaktoak Lagoon since records began in 1986 also occurred in 2016.

Recent attention has been given to how the Arctic and lower latitudes exchange mass and energy in an effort to better understand impacts of the phenomenon referred to as Arctic amplification, and in particular for improving predictions of potential changes in midlatitude weather patterns, but

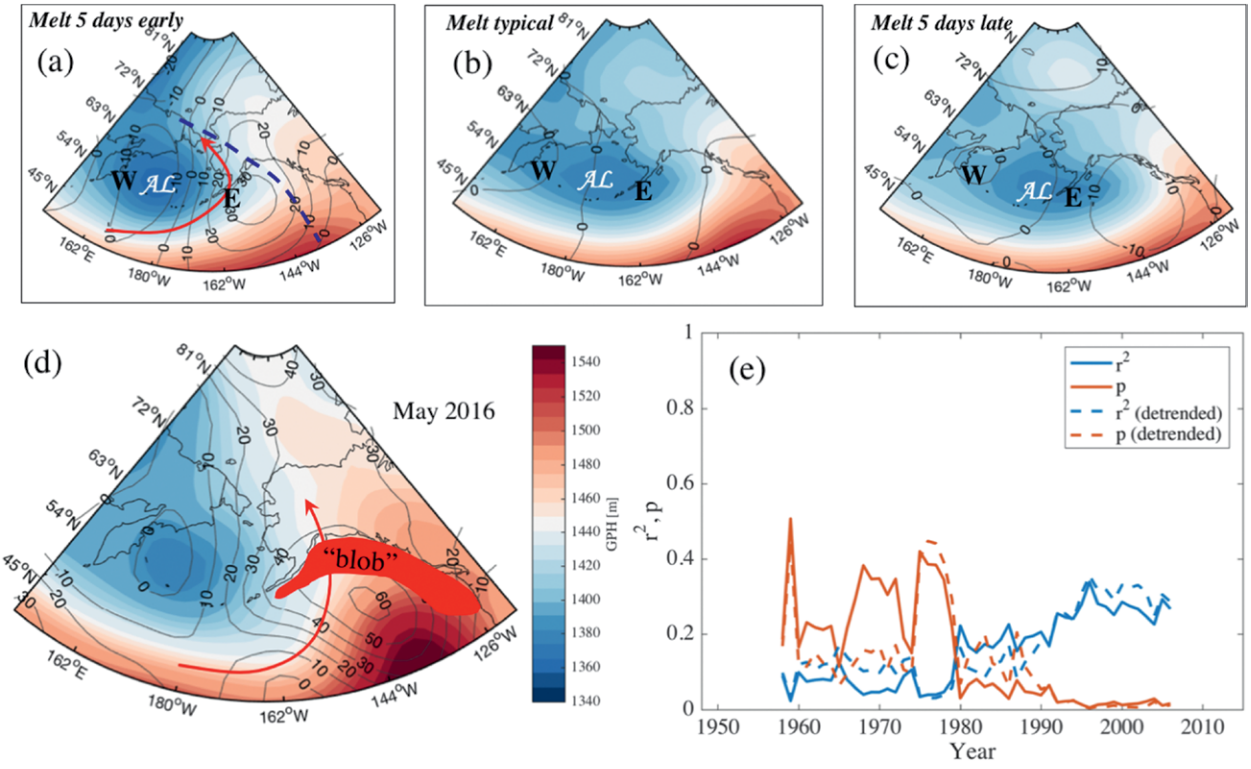

FIG. 7. May 850-hPa geopotential height (GPH) fields for years when snowmelt at BRW was (a) ≥5 days earlier than the 1948–2016 average [the red arrow shows the direction of airflow around the Aleutian low (AL), guided by a high pressure ridge represented by the dashed line], (b) ±4 days of average, and (c) ≥5 days later than average. Contour lines in (a)–(c) show the same pattern as the filled contours, but for the anomaly instead of the mean. An index that relates to the position and strength of the AL is calculated as the difference in geopotential height at 850 hPa for points, EW, where E is 55°N, 150°W and W is 55°N, 160°E as denoted in (a)–(c). (d) The average 850-hPa GPH for May 2016: the direction of airflow and the approximate position of the warm anomaly in the Gulf of Alaska (referred to as the "blob") are highlighted. (e) Coefficient of determination r^2 and associated p value for running 20-yr regressions between the date of melt at BRW and EW in May (solid lines); results are given also when both time series are linearly detrended (dashed).

answers remain elusive (Overland et al. 2015 and references therein). On a year-to-year basis, meteorological data from Utqiaġvik point to a significant and direct influence from lower latitudes on the temperature at Utqiaġvik during spring, signaling a dominance of large-scale processes over local processes in determining the timing of snowmelt. Conversely, in autumn, regional sea ice conditions are a dominant factor influencing the Utqiaġvik temperature patterns. Thus, looking forward, temperature and atmospheric circulation anomalies in the North Pacific may prove useful in creating statistical forecasts of spring snowmelt conditions with lead times of weeks to months, while variability in the summer sea ice melt season may foreshadow the timing of the arrival of snowpack. The development of statistical prediction tools for snow cover in the Alaskan region is important for seasonal planning of stakeholders including civil, industry, and natural resource managers. However, more work is needed to develop and refine predictive tools, especially in light of the likelihood of nonlinearity in long-term changes, or regime shifts associated with both tipping points and internal variability.

ACKNOWLEDGMENTS. The authors appreciate the efforts of Ross Burgener, Matthew Martinsen, Christine Schultz, Bryan Thomas, and Jim Wendell (all of NOAA GMD) in data collection, processing, and archival at BRW, Kamel Didan (The University of Arizona) for NDVI consultation, David Robinson (Rutgers) for insights into satellite-derived snow cover, and Gijs de Boer (NOAA/CIRES) for useful discussions of BRW and Oliktok data. Allison McComiskey (NOAA GMD), Taneil Uttal (NOAA PSD), and three anonymous reviewers provided helpful suggestions for improving the manuscript. C. Cox was supported by the Arctic Research Program (ARP) of the NOAA Climate Program Office (CPO). BRW data are available from NOAA GMD at www.esrl.noaa.gov/gmd/obop/brw/. Data collected by the U.S. Department of Energy ARM program may be acquired from www.arm.gov. National Weather Service (NWS) data are available from the NOAA/National Centers for Environmental Information (NCEI) at www.ncdc.noaa.gov/; data from 1902 to 1919 were collected by the NWS Cooperative Observer Program (COOP). Streamflow data for the Kuparuk (gauge 1586000, 70°16′54″N, 148°57′35″W) are from the USGS National Streamflow Information Program (NSIP) and maintained by the USGS Alaska Water Science Center, available from the USGS National Water Information System (NWIS) at https://waterdata.usgs.gov/nwis. Melt dates from SMMR and SSM/I passive microwave data from Markus et al. (2009) are available at https://neptune.gsfc.nasa.gov. Northern Hemisphere Snow Cover Extent (NH-SCE) data (Robinson et al. 2012; Estilow et al. 2015) are available from https://gis.ncdc.noaa.gov/. Niño-3.4 indices were acquired from the Global Climate Observing System (GCOS) Working Group on Surface Pressure at www.esrl.noaa.gov/psd/gcos_wgsp/Timeseries/Nino34/. SST data are from the NOAA Extended Reconstruction SST v4, available at www.esrl.noaa.gov/psd/data/gridded/data.noaa.ersst.v4.html. Vegetation phenology dates are from the VIPPEN_NDVI Version 4 dataset produced by the The University of Arizona's Vegetation Index and Phenology Lab, and archived at https://lpdaac.usgs.gov/. All data on black guillemots by the nonprofit NGO, Friends of Cooper Island (www.cooperisland.org/).

REFERENCES

Amaya, D. J., N. E. Bond, A. J. Miller, and M. J. DeFlorio, 2016: The evolution and known atmospheric forcing mechanisms behind the 2013–2015 North Pacific warm anomalies. *U.S. CLIVAR Variations*, No. 14, International CLIVAR Project Office, Southampton, United Kingdom, 1–6.

Atwood, T. C., E. Peacock, M. A. McKinney, K. Lillie, R. Wilson, D. C. Douglas, S. Miller, and P. Terletzky, 2016: Rapid environmental change drives increased land use by an Arctic marine predator. *PLoS One*, **11**, e0155932, https://doi.org/10.1371/journal.pone.0155932.

Bhatt, U. S., and Coauthors, 2010: Circumpolar Arctic tundra vegetation change is linked to sea ice decline. *Earth Interact.*, **14**, 1–20, https://doi.org/10.1175/2010EI315.1.

——, and Coauthors, 2013: Recent declines in warming and vegetation greening trends over pan-Arctic tundra. *Remote Sens.*, **5**, 4229–4254, https://doi.org/10.3390/rs5094229.

Bieniek, P. A., and Coauthors, 2015: Climate drivers linked to changing seasonality of Alaska coastal tundra vegetation productivity. *Earth Interact.*, **19**, 1–29, https://doi.org/10.1175/EI-D-15-0013.1.

Bond, N. E., M. F. Cronin, H. Freeland, and N. Mantua, 2015: Causes and impacts of the 2014 warm anomaly in the NE Pacific. *Geophys. Res. Lett.*, **42**, 3414–3420, https://doi.org/10.1002/2015GL063306.

Brook, R. W., J. O. Leafloor, K. F. Abraham, and D. C. Douglas, 2015: Density dependence and phenological mismatch: Consequences for growth and survival of sub-Arctic nesting Canada Geese. *Avian Conserv. Ecol.*, **10**, 1, https://doi.org/10.5751/ACE-00708-100101.

Brown, R. D., and D. A. Robinson, 2011: Northern Hemisphere spring snow cover variability and change over

1922–2010 including an assessment of uncertainty. *The Cryosphere*, **5**, 219–229, https://doi.org/10.5194/tc-5-219-2011.

Carpenter, L. J., and S. Reimann, 2014: Update on ozone-depleting substances (ODSs) and other gases of interest to the Montreal Protocol. Scientific assessment of ozone depletion: 2014, Global Ozone Research and Monitoring Project Rep. 55, World Meteorological Organization, 1.1–1.101. [Available online at www.esrl.noaa.gov/csd/assessments/ozone/2014/chapters/2014OzoneAssessment.pdf.]

Cavalieri D. J., C. L. Parkinson, P. Gloersen, and H. Zwally, 1996: Sea ice concentrations from Nimbus-7 SMMR and DMSP SSM/I-SSMIS passive microwave data. National Snow and Ice Data Center, Boulder, CO, accessed 16 June 2015, digital media, https://doi.org/10.5067/8GQ8LZQVL0VL.

Cochran, P., O. H. Huntington, C. Pungowiyi, S. Tom, F. S. Chapin III, H. P. Huntington, N. G. Maynard, and S. F. Trainor, 2013: Indigenous frameworks for observing and responding to climate change in Alaska. *Climatic Change*, **120**, 557–567, https://doi.org/10.1007/s10584-013-0735-2.

Cox, C. J., T. Uttal, C. N. Long, M. D. Shupe, R. S. Stone, and S. Starkweather, 2016: The role of springtime Arctic clouds in determining autumn sea ice extent. *J. Climate*, **29**, 6581–6596, https://doi.org/10.1175/JCLI-D-16-0136.1.

Curtis, J., G. Wendler, R. Stone, and E. Dutton, 1998: Precipitation decrease in the western Arctic, with special emphasis on Barrow and Barter Island, Alaska. *Int. J. Climatol.*, **18**, 1687–1707, https://doi.org/10.1002/(SICI)1097-0088(199812)18:15<1687::AID-JOC341>3.0.CO;2-2.

Derksen, C., and R. Brown, 2012: Spring snow cover extent reductions in the 2008–2012 period exceeding climate model projections. *Geophys. Res. Lett.*, **39**, L195504, https://doi.org/10.1029/2012GL053387.

Didan, K., and A. Barreto, 2016: NASA MEaSUREs Vegetation Index and Phenology (VIP) phenology NDVI yearly global 0.05deg CMG V004. NASA EOSDIS Land Processes DAAC, accessed 20 October 2015, https://doi.org/10.5067/MEaSUREs/VIP/VIPPHEN_NDVI.004.

Di Lorenzo, E., and N. Mantua, 2016: Multi-year persistence of the 2014/15 North Pacific marine heatwave. *Nat. Climate Change*, **6**, 1042–1048, https://doi.org/10.1038/nclimate3082.

Divoky, G. J., 1998: Factors affecting the growth of a Black Guillemot colony in northern Alaska. Ph.D. dissertation, University of Alaska Fairbanks, 144 pp. [Available online at https://scholarworks.alaska.edu/handle/11122/7488.]

——, G. E. Watson, and J. C. Bartonek, 1974: Breeding of the Black Guillemot in northern Alaska. *Condor*, **76**, 339–343, https://doi.org/10.2307/1366350.

——, P. M. Lukacs, and M. L. Druckenmiller, 2015: Effects of recent decreases in arctic sea ice on an ice-associated marine bird. *Prog. Oceanogr.*, **136**, 151–161, https://doi.org/10.1016/j.pocean.2015.05.010.

——, D. C. Douglas, and I. J. Stenhouse, 2016: Arctic sea ice a major determinant in Mandt's black guillemot movement and distribution during non-breeding season. *Biol. Lett.*, **12**, 20160275, https://doi.org/10.1098/rsbl.2016.0275.

Doiron, M., G. Gauthier, and E. Lévesque, 2015: Trophic mismatch and its effects on the growth of young in an Arctic herbivore. *Global Change Biol.*, **21**, 4364–4376, https://doi.org/10.1111/gcb.13057.

Dong, X., B. Xi, K. Crosby, C. N. Long, R. S. Stone, and M. D. Shupe, 2010: A 10 year climatology of Arctic cloud fraction and radiative forcing at Barrow, Alaska. *J. Geophys. Res.*, **115**, D17212, https://doi.org/10.1029/2009JD013489.

——, B. J. Zib, B. Xi, R. Stanfield, Y. Deng, X. Zhang, B. Lin, and C. N. Long, 2014: Critical mechanisms for the formation of extreme arctic sea-ice extent in the summers of 2007 and 1996. *Climate Dyn.*, **43**, 53–70, https://doi.org/10.1007/s00382-013-1920-8.

Druckenmiller, M. L., H. Eicken, J. C. George, and L. Brower, 2010: Assessing the shorefast ice: Iñupiat whaling trails off Barrow, Alaska. *SIKU: Knowing Our Ice: Documenting Inuit Sea Ice Knowledge and Use*, I. Krupnik et al., Eds., Springer, 203–228, https://doi.org/10.1007/978-90-481-8587-0_9.

Durant, J. M., D. Ø. Hjermann, G. Ottersen, and N. C. Stenseth, 2007: Climate and the match or mismatch between predator requirements and resource availability. *Climate Res.*, **33**, 271–283, https://doi.org/10.3354/cr033271.

Durner, G. M., and Coauthors, 2009: Predicting the future distribution of polar bear habitat in the polar basin from resource selection functions applied to 21st century general circulation model projections of sea ice. *Ecol. Monogr.*, **79**, 25–58, https://doi.org/10.1890/07-2089.1.

Dutton, E. G., and D. J. Endres, 1991: Date of snowmelt at Barrow, Alaska, U.S.A. *Arct. Alp. Res.*, **23**, 115–119, D17212, https://doi.org/10.2307/1551445.

Estilow, T. W., A. H. Young, and D. A. Robinson, 2015: A long-term Northern Hemisphere snow cover extent data record for climate studies and monitoring. *Earth Syst. Sci. Data*, **7**, 137–142, https://doi.org/10.5194/essd-7-137-2015.

Forbes, B. C., and Coauthors, 2016: Sea ice, rain-on-snow and tundra reindeer nomadism in Arctic Russia.

Biol. Lett., **12**, 20160466, https://doi.org/10.1098/rsbl.2016.0466.

Foster, J. L., 1989: The significance of the date of snow disappearance on the Arctic tundra as a possible indicator of climatic change. *Arct. Alp. Res.*, **21**, 60–70, https://doi.org/10.2307/1551517.

——, J. W. Winchester, and E. G. Dutton, 1992: The date of snow disappearance on the Arctic tundra as determined from satellite, meteorological station and radiometric in situ observations. *IEEE Trans. Geosci. Remote Sens.*, **30**, 793–798, https://doi.org/10.1109/36.158874.

Government of Yukon, 2015: State of the environment interim report - 2015: An update on environmental indicators. Government of Yukon State of the Environment Interim Rep., 43 pp, www.env.gov.yk.ca/publications-maps/documents/SOE_2015.pdf.

Graversen, R. G., T. Mauritsen, S. Drijfhout, M. Tjernström, and S. Mårtensson, 2011: Warm winds from the Pacific caused extensive Arctic sea-ice melt in summer 2007. *Climate Dyn.*, **36**, 2103–2112, https://doi.org/10.1007/s00382-010-0809-z.

Griffith, B., and Coauthors, 2002: The Porcupine caribou herd. Arctic Refuge coastal plain terrestrial wildlife research summaries, D. C. Douglas, P. E. Reynolds, and E. B. Rhode, Eds., U.S. Geological Survey Biological Science Rep. USGS/BRD/BSR-2002-0001, 8–37.

Hall, B. D., and Coauthors, 2011: Improving measurements of SF6 for the study of atmospheric transport and emissions. *Atmos. Meas. Tech.*, **4**, 2441–2451, https://doi.org/10.5194/amt-4-2441-2011.

Hare, S. R., and N. J. Mantua, 2000: Empirical evidence for North Pacific regime shifts in 1977 and 1989. *Prog. Oceanogr.*, **47**, 103–145, https://doi.org/10.1016/S0079-6611(00)00033-1.

Hinkel, K. M., and F. E. Nelson, 2003: Spatial and temporal patterns of active layer thickness at Circumpolar Arctic Layer Monitoring (CALM) sites in northern Alaska, 1995–2000. *J. Geophys. Res.*, **108**, 8168, https://doi.org/10.1029/2001JD000927.

——, and ——, 2007: Anthropogenic heat island at Barrow, Alaska, during winter: 2001–2005. *J. Geophys. Res.*, **112**, D06118, https://doi.org/10.1029/2006JD007837.

Hinzman, L. D., and Coauthors, 2005: Evidence and implications of recent climate change in northern Alaska and other Arctic regions. *Climatic Change*, **72**, 251–298, https://doi.org/10.1007/s10584-005-5352-2.

Hurrell, J. W., 2017: North Pacific (NP) index by Trenberth and Hurrell; monthly and winter. The Climate Data Guide, accessed 21 April 2017. [Available online at https://climatedataguide.ucar.edu/climate-data/north-pacific-np-index-trenberth-and-hurrell-monthly-and-winter.]

Kalnay, E., and Coauthors, 1996: The NCEP/NCAR 40-Year Reanalysis Project. *Bull. Amer. Meteor. Soc.*, **77**, 437–471, https://doi.org/10.1175/1520-0477(1996)077<0437:TNYRP>2.0.CO;2.

Kapsch, M.-L., R. G. Graversen, and M. Tjernström, 2013: Springtime atmospheric energy transport and the control of Arctic summer sea-ice extent. *Nat. Climate Change*, **3**, 744–748, https://doi.org/10.1038/nclimate1884.

Khan, M. A. H., M. E. Whelan, and R. C. Rhew, 2012: Effects of temperature and soil moisture on methyl halide and chloroform fluxes from drained peatland pasture soils. *J. Environ. Monit.*, **14**, 241–249, https://doi.org/10.1039/C1EM10639B.

Kim, Y., J. S. Kimball, K. Zhang, K. Didan, I. Velicogna, and K. C. McDonald, 2014: Attribution of divergent northern vegetation growth responses to lengthening non-frozen seasons using satellite optical-NIR and microwave remote sensing. *Int. J. Remote Sens.*, **35**, 3700–3721, https://doi.org/10.1080/01431161.2014.915595.

Kintisch, E., 2015: 'The Blob' invades Pacific, flummoxing climate change experts. *Science*, **348**, 17–18, https://doi.org/10.1126/science.348.6230.17.

Kovacs, K. M., C. Lydersen, J. E. Overland, and S. E. Moore, 2011: Impacts of changing sea-ice conditions on Arctic marine mammals. *Mar. Biodiversity*, **41**, 181–194, https://doi.org/10.1007/s12526-010-0061-0.

Li, J., K. Fan, and Z. Xu, 2016: Links between the late wintertime North Atlantic Oscillation and springtime vegetation growth over Eurasia. *Climate Dyn.*, **46**, 987–1000, https://doi.org/10.1007/s00382-015-2627-9.

Liebezeit, J. R., K. E. B. Gurney, M. Budde, S. Zack, and D. Ward, 2014: Phenological advancement in arctic bird species: Relative importance of snow melt and ecological factors. *Polar Biol.*, **37**, 1309–1320, https://doi.org/10.1007/s00300-014-1522-x.

MacLean, S. F., Jr., and N. A. M. Verbeek, 1968: Nesting of the Black Guillemot at Point Barrow. *Auk*, **85**, 139–140, https://doi.org/10.2307/4083642.

Markus, T., J. C. Stroeve, and J. Miller, 2009: Recent changes in Arctic sea ice melt onset, freezeup, and melt season length. *J. Geophys. Res.*, **114**, C12024, https://doi.org/10.1029/2009JC005436.

Mioduszewski, J., A. K. Rennermalm, D. A. Robinson, and L. Wang, 2015: Controls on spatial and temporal variability in Northern Hemisphere terrestrial snow melt timing, 1979–2012. *J. Climate*, **28**, 2136–2153, https://doi.org/10.1175/JCLI-D-14-00558.1.

Moore, S. E., and H. P. Huntington, 2008: Arctic marine mammals and climate change: Impacts and resilience. *Ecol. Appl.*, **18**, S157–S165, https://doi.org/10.1890/06-0571.1.

Mortin, J., G. Svensson, R. G. Graversen, M.-L. Kapsch, J. C. Stroeve, and L. N. Boisvert, 2016: Melt onset over Arctic sea ice controlled by atmospheric moisture transport. *Geophys. Res. Lett.*, **43**, 6636–6642, https://doi.org/10.1002/2016GL069330.

Outcalt, S. I., F. E. Nelson, and K. M. Hinkel, 1990: The zero-curtain effect: Heat and mass transfer across an isothermal region in freezing soil. *Water Resour. Res.*, **26**, 1509–1516, https://doi.org/10.1029/WR026i007p01509.

Overland, J., J. A. Francis, R. Hall, E. Hanna, S.-J. Kim, and T. Vihma, 2015: The melting Arctic and midlatitude weather patterns: Are they connected? *J. Climate*, **28**, 7917–7932, https://doi.org/10.1175/JCLI-D-14-00822.1.

Persson, P. O. G., 2012: Onset and end of the summer melt season over sea ice: Thermal structure and surface energy perspective from SHEBA. *Climate Dyn.*, **39**, 1349–1371, https://doi.org/10.1007/s00382-011-1196-9.

——, C. W. Fairall, E. L. Andreas, P. S. Guest, and D. K. Perovich, 2002: Measurements near the Atmospheric Surface Flux Group tower at SHEBA: Near-surface conditions and surface energy budget. *J. Geophys. Res.*, **107**, 8045, https://doi.org/10.1029/2000JC000705.

Prowse, T. D., F. J. Wrona, J. D. Reist, J. J. Gibson, J. E. Hobbie, L. M. J. Lévasque, and W. F. Vincent, 2006: Climate change effects on hydroecology of Arctic freshwater ecosystems. *Ambio*, **35**, 347–358, https://doi.org/10.1579/0044-7447(2006)35[347:CCEOHO]2.0.CO;2.

Rhew, R. C., Y. A. Teh, T. Abel, A. Atwood, and O. Mazéas, 2008: Chloroform emissions from the Alaskan Arctic tundra. *Geophys. Res. Lett.*, **35**, L21811, https://doi.org/10.1029/2008GL035762.

Robinson, D. A., and Coauthors, 2012: NOAA Climate Data Record (CDR) of Northern Hemisphere (NH) snow cover extent (SCE), version 1. NOAA National Climatic Data Center, accessed 2 December 2015, https://doi.org/10.7289/V5N014G9.

Rode, K. D., C. T. Robbins, L. Nelson, and S. C. Amstrup, 2015a: Can polar bears use terrestrial foods to offset lost ice-based hunting opportunities? *Front. Ecol. Environ.*, **13**, 138–145, https://doi.org/10.1890/140202.

——, R. R. Wilson, E. V. Regehr, M. St. Martin, D. C. Douglas, and J. Olson, 2015b: Increased land use by Chukchi Sea polar bears in relation to changing sea ice conditions. *PLoS One*, **10**, e0142213, https://doi.org/10.1371/journal.pone.0142213.

Romanovsky, V., M. Burgess, S. Smith, K. Yoshikawa, and J. Brown, 2002: Permafrost temperature records: Indicators of climate change. *Eos, Trans. Amer. Geophys. Union*, **83**, 589–594, https://doi.org/10.1029/2002EO000402.

Semmens, K. A., J. Ramage, A. Bartsch, and G. E. Liston, 2013: Early snowmelt events: Detection, distribution, and significance in a major sub-arctic watershed. *Environ. Res. Lett.*, **8**, 014020, https://doi.org/10.1088/1748-9326/8/1/014020.

Serreze, M. C., A. P. Barrett, J. C. Stroeve, D. N. Kindig, and M. M. Holland, 2009: The emergence of surface-based Arctic amplification. *Cryosphere*, **3**, 11–19, https://doi.org/10.5194/tc-3-11-2009.

Shiklomanov, N. I., D. A. Streletskiy, F. E. Nelson, R. D. Hollister, V. E. Romanivsky, C. E. Tweedie, J. G. Bockheim, and J. Brown, 2010: Decadal variations of active-layer thickness in moisture-controlled landscapes, Barrow, Alaska. *J. Geophys. Res.*, **115**, G00I04, https://doi.org/10.1029/2009JG001248.

Shupe, M. D., 2011: Clouds at Arctic atmospheric observatories. Part II: Thermodynamic phase characteristics. *J. Appl. Meteor. Climatol.*, **50**, 645–661, https://doi.org/10.1175/2010JAMC2468.1.

——, V. P. Walden, E. Eloranta, T. Uttal, J. R. Campbell, S. M. Starkweather, and M. Shiobara, 2011: Clouds at Arctic atmospheric observatories. Part I: Occurrence and macrophysical properties. *J. Appl. Meteor. Climatol.*, **50**, 626–644, https://doi.org/10.1175/2010JAMC2467.1.

Silk, P. J., G. C. Lonergan, T. L. Arsenault, and C. D. Boyle, 1997: Evidence of natural organochlorine formation in peat bogs. *Chemosphere*, **35**, 2865–2880, https://doi.org/10.1016/S0045-6535(97)00347-0.

Sterk, H. A. M., G. J. Steeneveld, and A. A. M. Holtslag, 2013: The role of snow-surface coupling, radiation, and turbulent mixing in modeling a stable boundary layer over Arctic sea ice. *J. Geophys. Res. Atmos.*, **118**, 1199–1217, https://doi.org/10.1002/jgrd.50158.

Stern, H. L., and K. L. Laidre, 2016: Sea-ice indicators of polar bear habitat. *Cryosphere Discuss.*, **10**, 2027–2041, https://doi.org/10.5194/tc-10-2027-2016.

Stien, A., and Coauthors, 2012: Congruent responses to weather variability in high arctic herbivores. *Biol. Lett.*, **8**, 1002–1005, https://doi.org/10.1098/rsbl.2012.0764.

Stone, R. S., 1997: Variations in western Arctic temperatures in response to cloud radiative and synoptic-scale influences. *J. Geophys. Res.*, **102**, 21 769–21 776, https://doi.org/10.1029/97JD01840.

——, E. G. Dutton, J. M. Harris, and D. Longenecker, 2002: Earlier spring snowmelt in northern Alaska as

an indicator of climate change. *J. Geophys. Res.*, **107**, 4089, https://doi.org/10.1029/2000JD000286.

——, D. C. Douglas, G. I. Belchansky, S. D. Drobot, and J. Harris, 2005: Correlated declines in Pacific Arctic snow and sea ice cover. *Arct. Res. U. S.*, **19**, 18–25.

Stroeve, J. C., M. C. Serreze, M. M. Holland, J. E. Kay, J. Maslanik, and A. P. Barrett, 2012: The Arctic's rapidly shrinking sea ice cover: A research synthesis. *Climatic Change*, **110**, 1005–1027, https://doi.org/10.1007/s10584-011-0101-1.

——, T. Markus, L. Boisvert, J. Miller, and A. Barrett, 2014: Changes in Arctic melt season and implications for sea ice loss. *Geophys. Res. Lett.*, **41**, 1216–1225, https://doi.org/10.1002/2013GL058951.

Sweeney, C., and Coauthors, 2016: No significant increase in long-term CH_4 emissions on North Slope of Alaska despite significant increase in air temperature. *Geophys. Res. Lett.*, **43**, 6604–6611, https://doi.org/10.1002/2016GL069292.

Trenberth, K. E., and J. W. Hurrell, 1994: Decadal atmosphere-ocean variations in the Pacific. *Climate Dyn.*, **9**, 303–319, https://doi.org/10.1007/BF00204745.

Tucker, C. J., 1979: Red and photographic infrared linear combinations for monitoring vegetation. *Remote Sens. Environ.*, **8**, 127–150, https://doi.org/10.1016/0034-4257(79)90013-0.

Uttal, T., and Coauthors, 2016: International Arctic Systems for Observing the Atmosphere: An International Polar Year legacy consortium. *Bull. Amer. Meteor. Soc.*, **97**, 1033–1056, https://doi.org/10.1175/BAMS-D-14-00145.1.

Wang, M., and J. E. Overland, 2015: Projected future duration of the sea-ice-free season in the Alaskan Arctic. *Prog. Oceanogr.*, **136**, 50–59, https://doi.org/10.1016/j.pocean.2015.01.001.

Wang, T., S. Peng, C. Ottlé, and P. Ciais, 2015: Spring snow cover deficit controlled by intraseasonal variability of the surface energy fluxes. *Environ. Res. Lett.*, **10**, 024018, https://doi.org/10.1088/1748-9326/10/2/024018.

Ward, D. H., J. Helmericks, J. W. Hupp, L. McManus, M. Budde, D. C. Douglas, and K. D. Tape, 2016: Multi-decadal trends in spring arrival of avian migrants to the central Arctic coast of Alaska: Effects of environmental and ecological factors. *J. Avian Biol.*, **47**, 197–207, https://doi.org/10.1111/jav.00774.

Wendler, G., M. Shulski, and B. Moore, 2010: Changes in the climate of the Alaskan North Slope and the ice concentration of the adjacent Beaufort Sea. *Theor. Appl. Climatol.*, **99**, 67–74, https://doi.org/10.1007/s00704-009-0127-8.

——, B. Moore, and K. Galloway, 2014: Strong temperature increase and shrinking sea ice in Arctic Alaska. *Open Atmos. Sci. J.*, **8**, 7–15, https://doi.org/10.2174/1874282301408010007.

Westermann, S., J. Lüers, M. Langer, K. Piel, and J. Boike, 2009: The annual surface energy budget of a high-arctic permafrost site on Svalbard, Norway. *Cryosphere*, **3**, 245–263, https://doi.org/10.5194/tc-3-245-2009.

Wickersham, J., 1902: James A. Wickersham diary [04], February 12 to December 31, 1902. Alaska State Library, ASL-MS107-Diary04-1902, accessed 9 January 2016. [Available online at http://vilda.alaska.edu/cdm/singleitem/collection/cdmg21/id/3110/rec/6.]

Worton, D. R., W. T. Sturges, J. Schwander, R. Mulvaney, J.-M. Barnola, and J. Chappellaz, 2006: 20th century trends and budget implications of chloroform and related tri- and dihalomethanes inferred from firn air. *Atmos. Chem. Phys.*, **6**, 2847–2863, https://doi.org/10.5194/acp-6-2847-2006.

Zeng, H., G. Jia, and H. Epstein, 2011: Recent changes in phenology over the northern high latitudes detected from multi-satellite data. *Environ. Res. Lett.*, **6**, 045508, https://doi.org/10.1088/1748-9326/6/4/045508.

Zhu, Z., and Coauthors, 2016: Greening of the Earth and its drivers. *Nat. Climate Change*, **6**, 791–795, https://doi.org/10.1038/nclimate3004.

Zona, D., and Coauthors, 2016: Cold season emissions dominate the Arctic tundra methane budget. *Proc. Natl. Acad. Sci. USA*, **113**, 40–45, https://doi.org/10.1073/pnas.1516017113.

Science at Your Fingertips

AMS Journals are now optimized for viewing on your mobile device.

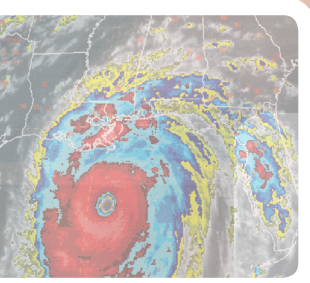

Access journal articles, monograph titles, and BAMS content using your iOS, Android, or Blackberry phone, or tablet.

Features include:

- **Saving articles for offline reading**
- **Sharing of article links via email and social networks**
- **Searching across journals, authors, and keywords**

And much more...

Scan code to connect to journals.ametsoc.org

AMERICAN METEOROLOGICAL SOCIETY